Nanoscale Advances

ROYAL SOCIETY OF CHEMISTRY

PAPER

View Article Online
View Journal | View Issue

Cite this: *Nanoscale Adv.*, 2023, **5**, 3053

Light-initiated aggregation of gold nanoparticles for synergistic chemo-photothermal tumor therapy†

Huawei Xia,‡[a] Jinfeng Zhu,‡[ab] Changhe Men,[a] Anna Wang,[a] Qiulian Mao,[a] Yali Feng,[a] Jiachen Li,[a] Jingwei Xu,[c] Xiaju Cheng*[a] and Haibin Shi *[a]

The combination of chemotherapy with photothermal therapy (PTT) has attracted extensive attention due to its excellent synergetic effect attributing to the fact that hyperthermia can effectively promote the tumor uptake of chemotherapeutic drugs. Herein, we propose a light-initiated gold nanoparticle (AuNP) aggregation boosting the uptake of chemotherapeutic drugs for enhanced chemo-photothermal tumor therapy. Novel light-responsive AuNPs (tm-AuNPs) were rationally designed and fabricated by conjugating both 2,5-diphenyltetrazole (Tz) and methacrylic acid (Ma) onto the surface of AuNPs with small size (~20 nm). Upon the irradiation of 405 nm laser, AuNPs could be initiated to form aggregates specifically within tumors through the covalent cycloaddition reaction between Tz and Ma. Taking advantage of the controllable photothermal effect of Au aggregates under NIR excitation, improved enrichment of doxorubicin (DOX) in tumor tissues was realized, combined with PTT, resulting in outstanding synergetic anti-tumor efficacy in living mice. We thus believe that this light-initiated AuNP aggregation approach would offer a valuable and powerful tool for precisely synergistic chemo-photothermal tumor therapy.

Received 23rd February 2023
Accepted 24th April 2023

DOI: 10.1039/d3na00114h

rsc.li/nanoscale-advances

Introduction

According to the latest global cancer report, cancer is still one of the major diseases that threaten human life and health,[1] although the mortality rate of cancer has presented a steady decrease in recent years owing to the improved diagnostic and therapeutic technology, especially the multi-modality combination treatment technique.[2–5] In general, multi-modality treatment can compensate the shortcomings of the single-modality approach with low efficiency and side effects to achieve synergistic enhancement of cancer therapy.[6–10] Chemotherapy is the most commonly used modality for tumor treatment in clinics. However, the unavoidable side effects of chemotherapeutic drugs to the body due to the poor tumor enrichment and undesired toxicity towards normal cells greatly affect the patient's life quality.[11–13] To overcome these problems, chemo-photothermal synergistic therapy has recently attracted wide attention in cancer treatment.[14–17]

Heat was documented to be used for breast cancer treatment thousands of years ago. It was termed as hyperthermia therapy, which is commonly defined as heating tissues at temperatures ranging from 42 to 55 °C.[18] Besides, hyperthermia has been demonstrated to be able to significantly enhance the cellular uptake of chemotherapeutic drugs in tumors because local heating can strengthen the damage of the cell membrane, tumor blood flow, and vascular permeability.[19–21] Nevertheless, it is difficult to realize the precise control of the temperature increase in the tumor region utilizing the conventional approaches, such as microwave, radiofrequency energy, ultrasound, *etc.*, in hyperthermia therapy.[22,23] Photothermal therapy (PTT) has drawn tremendous attention in the past few decades owing to the minimal invasiveness, excellent therapeutic efficiency, and great spatiotemporal addressability.[24–27] With the development of nanotechnology, many nanoagents with excellent PTT property have recently been applied for effective tumor treatment,[28–30] such as black phosphorus,[31,32] Bi_2S_3,[33] small molecule compounds[34] and gold nanomaterials. Among them, colloidal gold nanoparticles (AuNPs) are extensively recognized as promising PTT agents because of the feasible preparation, size uniformity, good biocompatibility, and tunable optical properties.[35–39] A large number of studies have demonstrated that small AuNPs with size less than 50 nm possess prolonged

[a]*State Key Laboratory of Radiation Medicine and Protection, School for Radiological and Interdisciplinary Sciences (RAD-X) and Collaborative Innovation Centre of Radiation Medicine of Jiangsu Higher Education Institutions, Soochow University, 199 Renai Road, Suzhou 215123, China. E-mail: xjcheng@suda.edu.cn; hbshi@suda.edu.cn*

[b]*Department of Experimental Medicine, TOR, University of Rome Tor Vergata, Roma 00133, Italy*

[c]*Department of Cardiothoracic Surgery, Suzhou Municipal Hospital Institution, Suzhou 215002, P. R. China*

† Electronic supplementary information (ESI) available. See DOI: https://doi.org/10.1039/d3na00114h

‡ Equal contribution.

blood circulation, shorter biological half-life, and deeper tissue penetration[40] compared to the large size of AuNPs that are readily entrapped by the reticuloendothelial system *in vivo*.[41] Whereas the local surface plasmon resonance (LSPR) peak of small AuNPs is usually located in the visible region, the ones of larger AuNPs are in the near infrared (NIR) region, which is the vital factor for the PTT effect.[42] To solve this contradiction, stimuli-responsive small AuNP aggregation approaches, including endogenous acidic pH,[43–46] cancer overexpression enzymes,[47–50] redox species[51,52] and exogenous temperature,[53] salt,[54] light,[55–59] *etc.*, have been successfully explored for PTT applications. However, the complexity of the tumor microenvironment often causes nonspecific AuNP aggregation leading to inevitable side effects on living systems.

In our previous work, we have successfully developed a light-initiated aggregation (LIA) strategy based on photocrosslinkable AuNPs for *in vivo* tumor PTT application.[55] Herein, to extend its wider applications in tumor theranostics *in vivo*, we rationally designed and fabricated a novel kind of light-responsive and crosslinkable gold nanoparticles (tm-AuNPs) by conjugating both 2,5-diphenyltetrazole (Tz) and methacrylic acid (Ma) groups onto the surface of small AuNPs. It was found that tm-AuNPs could be initiated to form aggregates specifically within tumors through the covalent cycloaddition reaction between Tz and Ma under the irradiation of a 405 nm laser (Scheme 1), which not only enhanced the accumulation and retention of AuNPs in tumor cells, but also produced a controllable photothermal effect at the tumor site upon NIR laser irradiation. Taking advantage of these unique properties of photocrosslinkable AuNPs, improved enrichment of doxorubicin (DOX) in tumor tissues was achieved, together with an excellent PTT effect, in consequence resulting in outstanding synergetic chemo-photothermal tumor therapy in living mice.

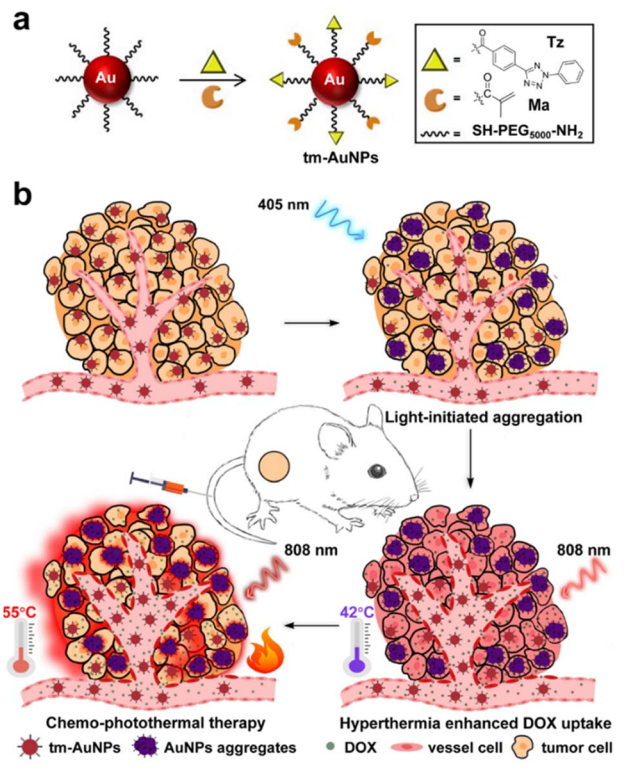

Scheme 1 Light-initiated aggregation of AuNPs for precisely synergistic chemo-photothermal tumor therapy. (a) Rational design and fabrication of tm-AuNPs. (b) Schematic illustration of *in vivo* synergistic chemo-photothermal tumor therapy with photocrosslinkable tm-AuNPs.

Experimental section

Materials

Chloroauric acid ($HAuCl_4 \cdot 3H_2O$), sodium citrate, 1-ethyl-3-(3′-dimethyl aminopropyl) carbodiimide (EDC), *N*-hydroxysuccinimide (NHS), 2,5-diphenyl tetrazole, methacrylic acid, and doxorubicin hydrochloride (DOX) were purchased from Sigma-Aldrich. Polyethylene glycol derivatives were bought from Beijing JenKem Technology Co., Ltd. The CCK-8 assay kit was bought from Dojindo Laboratories. The live/dead cell staining kit (Calcein-AM-PI) and the cell apoptosis kit (Annexin V-FITC/PI) were purchased from Invitrogen. Continuous wave (CW) 405 and 808 nm laser diodes were applied for photocrosslinking of tm-AuNPs and PTT, respectively.

Preparation of tm-AuNPs

Naked AuNPs (~20 nm) were first prepared by sodium citrate reduction of chloroauric acid according to the previously reported method.[37] CH_3O-PEG_{5000}-SH (20 mg) and NH_2-PEG_{5000}-SH (20 mg) were then added into 100 mL of AuNP aqueous solution and agitated for 12 h to afford NH_2-functionalized PEGylated AuNPs (AuNPs-PEG-NH_2). Meanwhile, EDC (6 mg) and NHS (10 mg) were dissolved in a DMSO solution containing 2,5-diphenyltetrazole acid (7 mg) and methacrylic acid (2 mg) and the solution was agitated for 20 min to activate the carboxylic group. After 20 min, AuNPs-PEG-NH_2 aqueous solution (1 mL, 2.48 mg mL^{-1}) was added into the reaction mixture followed by agitating at room temperature overnight, and then subjected to ultra-filtration in a centrifuge (5000 rpm) for 10 min to give the desired tm-AuNPs that were preserved at 4 °C for the subsequent experiments.

In vitro light-initiated aggregation of tm-AuNPs

To investigate the light-initiated aggregation of tm-AuNPs *in vitro*, tm-AuNP aqueous solution (50 μL, 1 mg mL^{-1}) was irradiated with 405 nm laser (1 W cm^{-2}) for 0, 5, 10, 15, 20, and 25 min. Meanwhile, the colloidal stability of AuNPs-PEG-NH_2 and tm-AuNPs with or without 405 nm laser irradiation was also determined. The light-triggered aggregation behavior of tm-AuNPs was monitored by DLS (Nano ZS90, Malvern), TEM (Tecnai G2 Spirit, FEI), and UV-vis absorption spectra measurements (UV-3600, Shimadzu).

In vitro photothermal therapeutic performance of AuNP aggregates

After 405 nm laser irradiation (1 W cm^{-2}, 25 min), the crosslinked AuNPs were diluted into a series of concentrations, *i.e.* 0, 20, 40, 80, 160 and 320 μg mL^{-1}, and then exposed to 808 nm

laser (0.75 W cm^{-2}, 10 min). Meanwhile, 100 μg mL^{-1} of crosslinked AuNPs was irradiated by an 808 nm laser with various power intensities (0, 0.5, 0.75, 1, and 1.5 W cm^{-2}) for 10 min. To evaluate the photothermal stability of AuNP aggregates, 100 μg mL^{-1} of AuNP aggregates was exposed to the 808 nm laser (0.75 W cm^{-2}) for 10 min, and then the machine was turned off to cool down to room temperature with three on/off cycles. A digital thermo imaging was used to monitor the real time temperature of AuNP aggregates upon 808 nm irradiation. The photothermal transfer efficiency was figured out with the following formula according to a previously reported method.[60,61]

$$\eta = \frac{mc(T_{max} - T_{max,H_2O})}{I(1 - 10^{-A})\tau_S}$$

where m is the solution weight, c is the heat capacity of water (4.2 J g^{-1}), T_{max} (55 °C) and $T_{max}\cdot H_2O$ (25 °C) are maximum temperatures achieved in the presence or absence of the cross-linked tm-AuNPs, I (1 W cm^{-2}) is the laser power density, A (1.2) is the absorbance of the cross-linked tm-AuNP solution at 808 nm, and τ_s is the system time constant (163.9 s).

Cytotoxicity detection of tm-AuNPs

Mouse breast cancer 4T1 cells were cultured with RPMI 1640 medium containing 10% fetal bovine serum and 1% penicillin streptomycin, and maintained in a damped 37 °C incubator with 5% CO_2. To investigate the cytotoxicity of tm-AuNPs, 5×10^3 cells per well density of 4T1 cells were grown in a 96-cell Petri dish. After growing for 24 h, the cells were incubated with different concentrations of tm-AuNPs (0, 25, 50, 100, and 200 μg mL^{-1}) for 24 h or 48 h. Then the cell survival was detected using the CCK-8 assay kit according to the manufacturer's instruction.

Light-initiated aggregation of tm-AuNPs in living cells

To evaluate the light-initiated aggregation of tm-AuNPs in living cells, 4T1 cells were grown in a 12-cell Petri dish with a thickness of 2×10^4 cells per well. After 24 h growth, the cells were incubated with 50 μg mL^{-1} of tm-AuNPs for 24 h, and then irradiated with or without 405 nm laser (1 W cm^{-2}) for 3 min. The medium was removed and the cells were washed twice with PBS. The end time of 405 nm laser irradiation was set as 0 h time point. After that, the cellular uptake of tm-AuNPs was detected at 6 and 12 h time points by dark field microscopy (Olympus, Tokyo, Japan).

In vitro PTT effect of tm-AuNPs

For live/dead staining assay, 2×10^4 4T1 cells per dish were seeded in a 12-cell Petri dish. After 24 h growth, cells were incubated with 80 μg mL^{-1} of tm-AuNPs for further 24 h. The cells were then exposed to 405 nm laser (1 W cm^{-2}) for 3 min followed by 808 nm irradiation (1 W cm^{-2}, 10 min), which are denoted as tm-AuNPs + λ_{405nm} + NIR. Five other groups were set as control (PBS), tm-AuNPs, λ_{405nm}, tm-AuNPs + λ_{405nm} (incubated with tm-AuNPs followed by 405 nm irradiation), and tm-AuNPs + NIR (incubated with tm-AuNPs followed by 808 nm irradiation). After that, the cells were incubated for further 24 h, and stained with Calcein-AM and propidium iodide for 30 min. The number of green live cells and red dead cells were imaged with fluorescence microscopy (20×). In addition, the PTT effect of tm-AuNPs was evaluated by the CCK-8 assay and apoptosis was analyzed by flow cytometry. The 4T1 cells were grown in a 96-cell Petri dish with a density of 5×10^3 cells per dish and subjected to different treatments as mentioned above. The cell viabilities of different treatment groups were evaluated by CCK-8 assays, and the percentage of apoptotic cells was detected by flow cytometry after staining with Annexin V-PE and 7-AAD.

Development of the tumor-bearing mice model

All animal studies were approved by the Animal Ethics Committee of Soochow University in accordance with the guidelines for the care and use of laboratory animals (approval number: 201802A088). Six weeks female BALB/c mice were bought from ChangZhou Cavensla Experimental Animal Technology Co. Ltd and fed under the standard environment (25 ± 2 °C/60 ± 10% relative humidity) with 12 h light/dark cycle. 1×10^6 4T1 cells were injected at the backside of the mouse. After the tumour volume grew up to about 100 mm^3, the mice were used for the subsequent *in vivo* experiments.

In vivo chemo-photothermal therapeutic effect of tm-AuNPs

We also evaluated the photothermal effect of tm-AuNPs *in vivo*. 1×10^6 4T1 cells were injected at the backside of the mouse. After the tumour volume grew up to about 100 mm^3, the mice were i.v. injected with tm-AuNPs (30 mg kg^{-1}). After 12 h, the tumors were irradiated with or without the 405 nm laser (1 W cm^{-2}, 25 min). Then we assessed the real-time local temperature increase of tumors upon two phases of 808 nm irradiation, namely, 0.5 W cm^{-2} for 30 min (denoted as HT) and 0.75 W cm^{-2} for 5 min (denoted as PT). Additionally, to investigate whether HT can enhance the chemotherapeutic efficacy, the mice were i.v. injected with tm-AuNPs (30 mg kg^{-1}) and DOX (2 mg kg^{-1}), and then exposed to 405 and 808 nm laser, respectively. After ~1 h, the tumors were extracted and sliced for fluorescence imaging.

To assess the chemo-photothermal synergistic therapeutic effect of tm-AuNPs *in vivo*, the tumor-bearing mice were classified into four groups including PBS + HT + PT (mice i.v. injected with PBS followed by two phases of 808 nm laser irradiation), tm-AuNPs + DOX + HT + PT (mice i.v. injected with tm-AuNPs and DOX followed by two phases of 808 nm laser irradiation), tm-AuNPs + λ_{405nm} + DOX + HT (mice i.v. injected with tm-AuNPs followed by 405 nm irradiation, then DOX and 808 nm irradiation with lower power), and tm-AuNPs + λ_{405nm} + DOX + HT + PT (mice i.v. injected with tm-AuNPs followed by 405 nm irradiation, then DOX and 808 nm irradiation with both low and high power) (tm-AuNPs = 30 mg kg^{-1}, DOX = 2 mg kg^{-1}, λ_{405nm} = 1 W cm^{-2} 405 nm laser for 25 min, HT = 0.5 W cm^{-2} 808 nm laser for 30 min, PT = 0.75 W cm^{-2} 808 nm laser for 5 min). After different treatments, the tumor size was measured with a caliper every day. The tumor volume was calculated as follows: $V = ab^2/2$, where a and b are the tumor

length and width, respectively. The tumors were extracted on the 3rd day post-treatment for H&E staining analysis.

Results and discussion

Fabrication and characterization of tm-AuNPs

In this work, novel light-responsive and crosslinkable gold nanoparticles, tm-AuNPs, were prepared according to the previously reported method.[62] Briefly, PEGylated AuNPs with –NH_2 (AuNPs-NH_2) on the surface were first prepared by decorating the thiol-poly(ethyleneglycol)-amine onto the surface of naked AuNPs. 2,5-Diphenyltetrazole (Tz) and methacrylic (Ma) groups were then conjugated to PEG ligands through the classical amidation reaction between carboxylic acid and –NH_2 mediated by EDC/NHS to afford the desired tm-AuNPs. The loading contents of Tz and Ma were detected by HPLC before and after reaction with Au-PEG-NH_2. According to the HPLC results in Fig. S1,† the molar ratio between PEG-NH_2, Tz, and Ma was calculated to be 4 : 2.3 : 1.5 on one single tm-AuNP based on the equation $n = m \times (1 - C_{after}/C_{before})/M$. The structures of resulting AuNPs were confirmed by both Fourier transform infrared,[62] and absorption analysis (Fig. S2†). Dynamic light scattering (DLS) results indicate that the hydrodynamic diameters of AuNPs-NH_2 and tm-AuNPs are 33.5 and 34 nm, respectively. Accordingly, their sizes were also measured by transmission electron microscopy (TEM) to be 21 and 23 nm (Fig. S3†). Moreover, both AuNPs-NH_2 and tm-AuNPs exhibited excellent stability in aqueous solution over 3 days at room temperature (Fig. S4†), indicating that they have great potential for biological applications.

It is well known that the tetrazole group can spontaneously undergo a photo-click reaction with the alkene dipolarophile moiety to form a cycloaddition product under the irradiation of UV light.[63,64] To evaluate the aggregating behavior of tm-AuNPs upon the irradiation of the 405 nm laser, the tm-AuNP aqueous solution was first exposed to the 405 nm laser (1 W cm^{-2}) for different irradiation times, and then monitored by TEM and DLS measurements. As shown in Fig. 1a, significant aggregation of tm-AuNPs occurred after 10 min of irradiation, and the degree of particle aggregates progressively increased in an irradiation time-dependent manner. Along with the morphological variation of particles, DLS data also showed that the hydrodynamic size of tm-AuNPs gradually increased from the initial 38 nm to 342 nm with the irradiation time increasing from 0 to 25 min (Fig. 1b). However, the size of AuNPs-NH_2 remained almost unchanged even with continuous illumination for up to 25 min (Fig. S4†). Meanwhile, the color of the tm-AuNP solution changed from the original wine red to purplish black. Moreover, the absorption spectra in Fig. 1c clearly show that the maximal absorption peak of the isolated tm-AuNPs was initially located at around 520 nm, while as the irradiation time was increased, the surface plasmon resonance absorbance at 520 nm gradually decreased accompanied by an evident red-shift and enhancement in the NIR region of 700–900 nm. Together, these results strongly demonstrate that the covalent interparticle crosslinking of tm-AuNPs can be effectively triggered by 405 nm laser irradiation through the cycloaddition reaction between Tz and Ma groups.

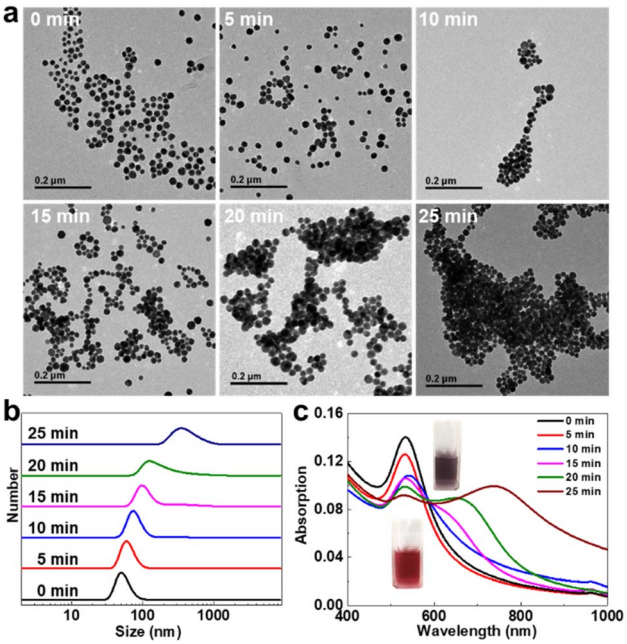

Fig. 1 Study of light-initiated aggregation of tm-AuNPs in aqueous solution. (a) TEM images, (b) hydrodynamic size, and (c) UV-vis-NIR absorption spectra of tm-AuNPs with or without 405 nm laser exposing different phases of time. (Inset of panel c: pictures of aqueous solutions of tm-AuNPs with or without laser irradiation for 25 min.)

Photothermal effect study of tm-AuNPs *in vitro*

Inspired by the strong NIR absorption of tm-AuNP aggregates, we next evaluated the photothermal performance of tm-AuNPs *in vitro*. The tm-AuNP aqueous solution was first exposed to a 405 nm laser (1 W cm^{-2}) for 25 min, and then diluted to different concentrations for the 808 nm laser (0.75 W cm^{-2}) with various irradiation times from 0 to 10 min followed by temperature monitoring. As shown in Fig. 2a, the temperature of the solutions containing the aggregated AuNPs gradually increased with the extension of irradiation time. The temperature increase displays a positive correlation with increased amounts of tm-AuNPs used. For the solution of tm-AuNPs (160 μg mL^{-1}) after 10 min irradiation, the temperature rose by up to 46.5 °C, while less than 2 °C of temperature increase was detected from water as a control. Besides, the degree of temperature increase was also positively enhanced along with the power density of 808 nm laser (Fig. 2b). These results strongly suggest that the light-initiated aggregation of tm-AuNPs possesses a great photothermal effect. Moreover, the photothermal stability of Au aggregates was also investigated. Fig. 2c shows that the temperature of the aggregated AuNP (100 μg mL^{-1}) solution could rise up to 55 °C under 808 nm laser irradiation (1 W cm^{-2}, 10 min), and remained unchanged for three on/off cycles. The photothermal conversion efficiencies (η) of crosslinked and non-crosslinked AuNPs were further

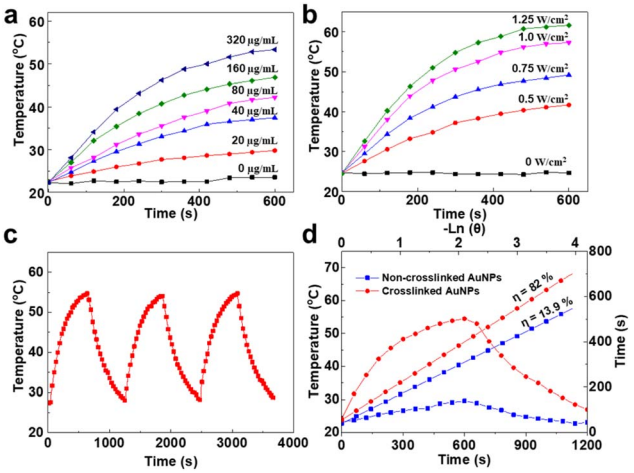

Fig. 2 *In vitro* characterization of the PTT effect. (a) Correlated heating curves of different concentrations of tm-AuNP aqueous solutions with the photo-crosslinking process upon 808 nm laser irradiation with a power density of 0.75 W cm^{-2} for 10 min, (b) correlated heating curves of the crosslinked AuNP solutions (100 μg mL^{-1}) under the irradiation of 808 nm laser irradiation with different power densities for 10 min, (c) temperature changes of the crosslinked AuNP solution (100 μg mL^{-1}) with three cycles of 808 nm laser on/off (1 W cm^{-2}, 10 min), (d) linear analysis of photothermal performance of the crosslinked AuNP solution by cooling to room temperature and plot of cooling time *versus* negative natural log of the temperature change.

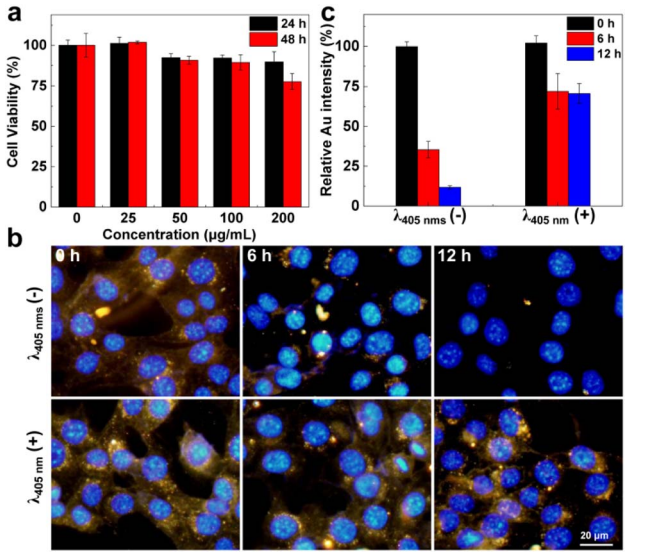

Fig. 3 *In vitro* cellular uptake of tm-AuNPs. (a) Cell viability of 4T1 cells after incubation with different concentrations of tm-AuNPs for 24 h or 48 h. (b and c) Dark field images and corresponding quantitative analysis of 4T1 cells after being incubated with tm-AuNPs for showing the longer retention time of nanoparticles induced by 405 nm irradiation compared to the cells without irradiation. [tm-AuNPs] = 50 μg mL^{-1}, 405 nm laser: 1 W cm^{-2}, t = 3 min.

calculated to be 82% and 13.9%, respectively (Fig. 2d). Collectively, all these results strongly demonstrated that tm-AuNPs can be triggered by the 405 nm laser to form covalently crosslinked nanoaggregates, and have great potential as PTT agents for tumor treatment application.

Light-initiated aggregation of tm-AuNPs in living cells

To further evaluate the light-initiated crosslinking behavior of tm-AuNPs in living cells, the cytotoxicity of tm-AuNPs towards mouse breast cancer cells 4T1 was first evaluated by the widely used Cell Counting Kit-8 (CCK-8) assay. As illustrated in Fig. 3a, the cells receiving 100 μg mL^{-1} of tm-AuNPs remained above 90% of overall cell viability both after 24 and 48 h incubation, indicating that tm-AuNPs have a negligible cytotoxicity towards 4T1 cells below 100 μg mL^{-1}. In light of the great biocompatibility of tm-AuNPs, we next studied the intracellular internalization behavior of tm-AuNPs. As shown in Fig. S5,† most of the Au nanoparticles were localized at intracellular endocytic vesicles in the cytoplasmic region. According to our previous study,[37] they were proposed to be internalized by cancer cells based on the caveolin-mediated endocytosis. Additionally, we investigated the light-initiated crosslinking performance of tm-AuNPs in 4T1 cells. Two groups of 4T1 cells were incubated with tm-AuNPs (50 μg mL^{-1}) for 24 h followed by irradiation with or without the 405 nm laser (1 W cm^{-2}, 3 min). The cellular contents of AuNPs were then real-time visualized by dark-field microscopy that can be adopted to represent the intensity of scattered light from AuNPs reflecting the contents of nanoparticles in living cells.[65] The microscopy images in Fig. 3b indicate that the intensity of AuNPs in the cells receiving photo-irradiation was obviously higher than the ones without irradiation whether at 6 h or 12 h post-irradiation. The light-initiated aggregation of tm-AuNPs in living cells was further confirmed by TEM. Obvious nanoaggregates were determined in 4T1 cells with 405 nm irradiation, while no aggregation was observed for the cells without irradiation. Additionally, the Au content in the cells without 405 nm irradiation rapidly decreased with the increase of incubation time. Only ~11% of original AuNPs were retained at 12 h post-irradiation, whereas the cells with 405 nm irradiation apparently showed a slower Au intensity decay with around 70% of original AuNPs preserved (Fig. 3c), implying that this light-initiated aggregation approach can effectively prolong the residence time of particles in living cells.

In vitro study of the photothermal therapeutic effect of tm-AuNPs

In light of the above intriguing results, the covalent crosslinking of AuNPs could on-demand occur under the stimulation of the 405 nm laser in living cells. To evaluate the photothermal effect of the resulting crosslinked AuNP aggregate, six groups of 4T1 cells were subjected to various combination treatments followed by live/dead cell staining. As shown in Fig. 4a, a large number of dead cells were apparently determined mainly from the tm-AuNP-treated cells that were sequentially irradiated by 405 nm (1 W cm^{-2}, 3 min) and 808 nm laser irradiation (0.75 W cm^{-2}, 10 min) (tm-AuNPs + λ_{405nm} + NIR). However, nearly no cell death was observed in the other five groups of cells (control, tm-AuNPs, λ_{405nm}, tm-AuNPs + λ_{405nm}, and tm-AuNPs + NIR) as controls. Their photothermal therapeutic efficacies on 4T1 cells

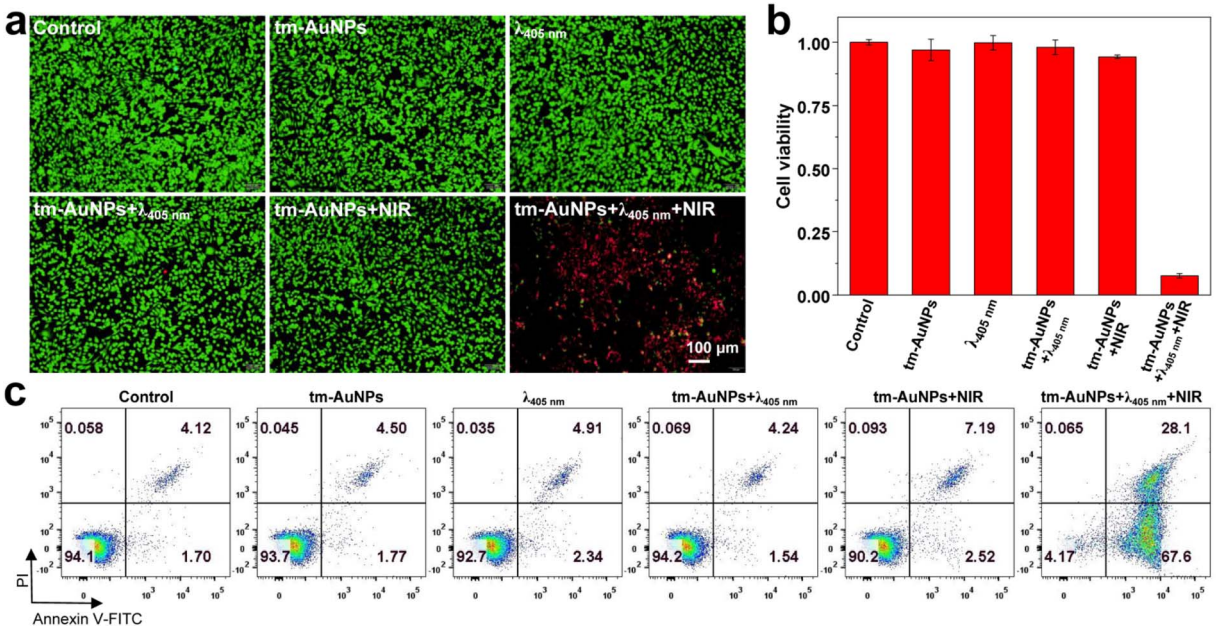

Fig. 4 Study of the photothermal effect of tm-AuNPs in living cells. (a) The live/dead staining of 4T1 cells with different combination treatments. (b) Cell viability characterization of 4T1 cells with different combination treatments in (a). (c) Cell apoptosis analysis of 4T1 cells with various treatments using flow cytometry.

were further quantitatively characterized by the CCK-8 assay as well as flow cytometry assays. Fig. 4b indicates that the cell viability of the tm-AuNPs + λ_{405nm} + NIR group was only 7.6%, while the other five control groups remained above 90%. Moreover, the flow cytometry analysis showed that the rates of early and later apoptosis in the cells of tm-AuNPs + λ_{405nm} + NIR was up to 67.6% and 28.1%, respectively, which is much higher than that in tm-AuNPs + NIR and other control cells (Fig. 4c), strongly demonstrating that the 405 nm irradiation is a crucial prerequisite for aggregation of tm-AuNPs in living cells achieving a remarkable photothermal therapeutic effect.

Synergistic chemo-photothermal therapy of tumors *in vivo*

Inspired by the above prominent photothermal effect of tm-AuNPs *in vitro*, we further explored the light-initiated aggregation performance of tm-AuNPs for *in vivo* synergistic chemo-photothermal therapy of tumors. We first investigated the blood circulation behavior of tm-AuNPs in 4T1 tumor-bearing mice. According to the single-component pharmacokinetic model, the blood half-life of tm-AuNPs was calculated to be 9.76 h (Fig. S6a†). Meanwhile, the biodistribution of tm-AuNPs was also evaluated by determining the Au content in various organs and tumor. The results indicate that the ID %/g value of the tumor is ~5.1% at 12 h post-injection of tm-AuNPs (Fig. S6b†). It has been well documented that hyperthermia can significantly enhance the cellular uptake of chemotherapeutic drugs in tumors because the mild heating (usually about 42 °C) of local tissues can accelerate the tumor blood vessel flow and permeability.[66,67] To validate the hyperthermia effect of AuNP aggregates for enhancement of drug uptake, we first monitored the cellular uptake of DOX in 4T1 cells under different treatments. As shown in Fig. S7,† the cellular uptake of DOX was remarkably enhanced if tumor cells were irradiated by the 808 nm laser (0.5 W cm^{-2}, 10 min), implying that the local temperature rise can promote the cellular uptake of DOX, which is quite consistent with that of previously reported studies.[68–70] Moreover, the synergistic chemo-photothermal effect of tm-AuNPs on 4T1 cells was quantitatively characterized by the CCK-8 assay and live/dead assay. The cell viabilities of tm-AuNPs + λ_{405nm} + HT and Dox + tm-AuNPs + λ_{405nm} groups were 87.53% and 78.68% (Fig. S8†), respectively, while the cell viability of the Dox + tm-AuNPs + λ_{405nm} + HT group was as low as 31.65%, and the combination index value was calculated to be 0.78 according to the previously reported method,[33] indicative of a moderate synergistic chemo-photothermal effect. Furthermore, 4T1 tumor-bearing mice were intravenously injected with tm-AuNPs (30 mg kg^{-1}) first, and the tumors were then irradiated with 405 nm to induce on-site AuNP aggregation followed by 808 nm irradiation. The hyperthermia (HT, 0.5 W cm^{-2} of irradiation for 30 min) and photothermal (PT, 1.0 W cm^{-2} of irradiation for 5 min) treatments of tumors were realized by controlling the power intensity and irradiation time of the 808 nm laser. As shown in Fig. 5a, the tumors with the photo-crosslinking process (tm-AuNPs + λ_{405nm}) clearly exhibited dramatic temperature increase upon continual 35 min of 808 nm laser irradiation compared to the ones without photo-crosslinking (tm-AuNPs and PBS). Real-time monitoring of the tumor temperature change indicated that all groups of tumors kept the local temperature below 42 °C during the HT stage. However, if the tumors were continually irradiated by the 808 nm laser with a power of 1.0 W cm^{-2} for further 5 min, only the tumors in the tm-AuNPs + λ_{405nm} group experienced

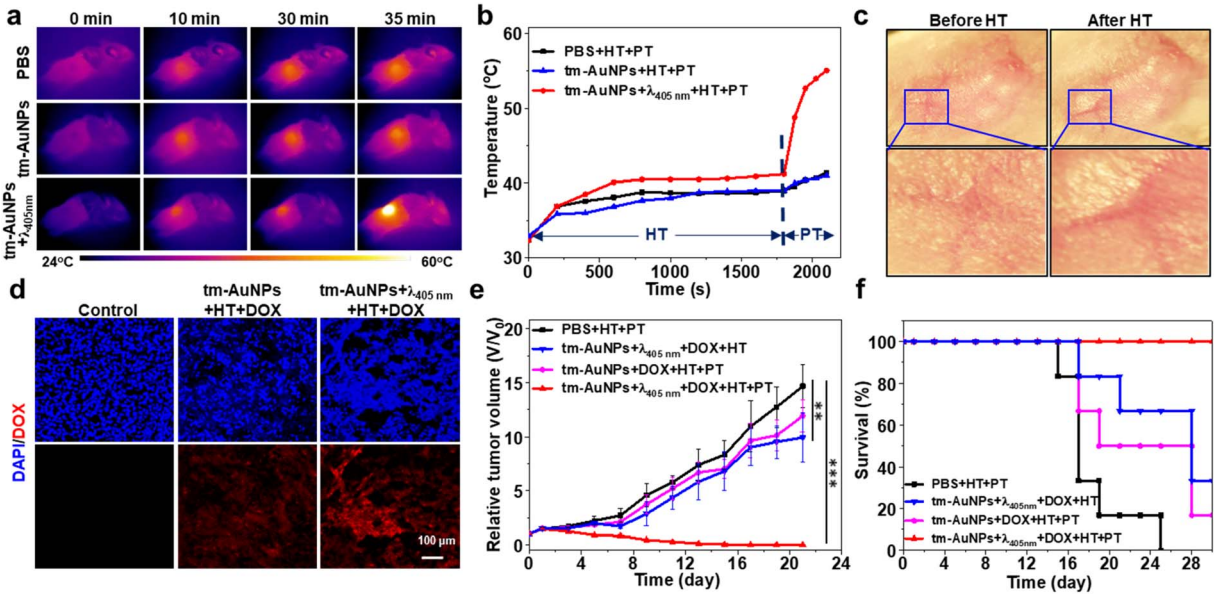

Fig. 5 *In vivo* study of the synergistic chemo-photothermal therapy of tumors. (a) Photothermal graphs of tumor-bearing mice with various combination treatments under 808 nm laser irradiation. (b) Real-time heating curves of tumors irradiated with 808 nm laser at 0.5 W cm^{-2} for 30 min and then at 0.75 W cm^{-2} for 10 min. (c) Photographs of local blood vessels in the tumor region for showing that the hyperthermia effect of crosslinked AuNPs under 808 nm can promote the tumor blood flow and vasodilation. (d) Fluorescence imaging of 4T1 tumor tissues for revealing the uptake of DOX. DAPI (blue) was used to stain the nuclei of frozen tumor sections. Red fluorescence is from DOX. (e) Relative tumor volume of mice receiving different combination treatments ($n = 4$). (f) Survival percentage of mice with different combination treatments.

a remarkable rise in local temperature up to 55 °C during the PT stage, whereas the other groups of tumors still remained below 42 °C (Fig. 5b). These results strongly demonstrate that the local temperature of tumors can be spatiotemporally controlled and regulated based on our strategy, which has great potential to improve the efficacy of conventional chemotherapeutic drugs in tumor treatment.

Doxorubicin (DOX) is one of the most commonly used chemotherapeutic drugs for cancer treatment in clinics. To investigate the feasibility of our LIA approach in improving the uptake of DOX in tumor tissues, we first conducted a study on the tumor uptake of DOX under the stimulation of the HT effect. 4T1 tumor-bearing mice were intravenously injected with tm-AuNPs (30 mg kg^{-1}) and then irradiated with or without 405 nm (1 W cm^{-2}) at 12 h post-injection followed by injection of DOX (2 mg kg^{-1}). The tumors were irradiated by exposure to 808 nm (0.5 W cm^{-2}) immediately for studying the effect of hyperthermia on drug uptake. We noticed that the local blood vessels in the tumor region were obviously dilated and blood flow was significantly increased after HT, implying that more drug will be accumulated in the tumor (Fig. 5c). To detect DOX in the tumor directly, the tumors receiving different treatments were subsequently dissected and sliced for *ex vivo* fluorescence imaging. Fig. 5d depicts that the tumors with tm-AuNPs + λ_{405nm} + HT exhibited obviously the highest red fluorescence emitted by DOX in comparison with the ones receiving PBS and tm-AuNPs + HT indicative of high DOX uptake, suggesting that the hyperthermia effect of the crosslinked AuNPs under 808 nm can effectively promote the enrichment of chemotherapeutic drugs in tumor tissues. Meanwhile, the tumor growth was evidently suppressed for the mice with tm-AuNPs + DOX + λ_{405nm} + HT compared to other control mice, demonstrating the excellent HT therapeutic performance of tm-AuNPs *in vivo* (Fig. S9a†). Nevertheless, the tumor growth is still hard to be completely suppressed. Additionally, the average body weights of all groups of mice show no apparent change during the treatment period of 13 days (Fig. S9b†). The tumor tissues and major organs were further dissected and sectioned for hematoxylin and eosin (H&E) staining. As expected, the tumors of tm-AuNPs + DOX + λ_{405nm} + HT showed the most severe malignant necrosis (Fig. S9c and d†), while no noticeable damage was determined for the major organs (Fig. S10†). Collectively, these results strongly demonstrate that our LIA approach can remarkably improve the therapeutic efficacy of chemotherapeutics *in vivo*.

Encouraged by the exciting finding that the hyperthermia effect of AuNP aggregates can remarkably improve the chemotherapeutic efficacy of tumors, we further assessed the chemo-photothermal combination therapeutic effect on tumors *in vivo*. Four groups of 4T1 tumor-bearing mice ($n = 4$) were subjected to different combination treatments followed by monitoring of the tumor size over 21 days. As shown in Fig. 5e, the tumor growth of the mice receiving tm-AuNPs + λ_{405nm} + DOX + HT and photothermal therapy (PTT) (808 nm laser at 0.75 W cm^{-2} for 10 min) (denoted as tm-AuNPs + λ_{405nm} + DOX + HT + PT) was effectively inhibited with a significant tumor suppression, suggesting that the mice have a great survival rate (Fig. 5f). However, only weak tumor suppression was determined for the other three control groups of mice with the treatments of PBS + HT + PT, tm-AuNPs + λ_{405nm} + DOX + HT, or tm-AuNPs + DOX +

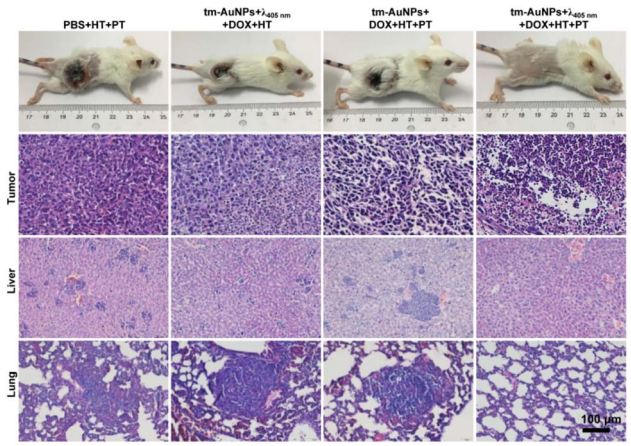

Fig. 6 Photographs of representative mice in each group and the tumors were extracted on the 3rd day post-treatment for H&E staining to demonstrate the therapeutic efficacy of different combination treatments, and H&E staining of liver and lung on the 30th day post-treatment.

HT + PT (Fig. S11†). In addition, no apparent weight change was determined for all groups of mice during the whole treatment period (Fig. S12a†). Moreover, the tumor tissues were extracted on 3rd day posttreatment for pathological analysis. In comparison to other controls, significant karyopyknosis and necroptosis were detected in the tumorous tissues of tm-AuNPs + λ_{405nm} + DOX + HT + PT (Fig. 6), revealing the excellent synergistic chemo-photothermal efficacy of light-responsive tm-AuNPs. Besides, H&E staining of major organ tissues on 30th day posttreatment indicates that apparent tumor metastasis was exclusively observed in the lung and liver of control mice (Fig. 6 and S12b†), which is quite consistent with previously mentioned survival rate results. To further assess the metabolism of gold nanoparticles *in vivo*, we measured the amount of AuNPs present in the body on the last day post-treatment. As shown in Fig. S12c,† the Au content in various organs and tumor was fairly less than 10%, suggesting that the Au aggregates can be eventually well excreted from the body. Collectively, all these proofs strongly demonstrate that our light-initiated AuNP aggregation approach could not only enhance the enrichment of DOX in tumors under NIR irradiation, but also achieve an efficient chemo-photothermal synergistic therapy of tumors *in vivo*.

Conclusions

In summary, we have successfully fabricated novel light-responsive AuNPs by incorporating 2,5-diphenyltetrazole and methacrylic acid onto the surface of gold nanoparticles for chemo-photothermal synergistic therapy of tumors. The tm-AuNPs could be on-demand triggered to form crosslinked particle aggregates at the tumor site under 405 nm irradiation through a tetrazole/alkene cycloaddition reaction resulting in prolonged retention and activated photothermal effect to enhance the uptake of DOX in tumors. More notably, taking advantage of the temperature controllability of Au aggregates, an effective tumor suppression was realized by the synergistic chemo-photothermal treatment. We thus believe that this innovative light-initiated aggregation approach may offer an attractive and powerful platform for effective chemo-photothermal synergistic cancer therapy.

Conflicts of interest

There are no conflicts to declare.

Acknowledgements

We acknowledge the financial support from the National Science Foundation of China (22077092, 81902913), the Training Program of the Major Research Plan of the National Natural Science Foundation of China (91959123), the Natural Science Foundation of Jiangsu Province (BK20190821), the Open Project Program of the State Key Laboratory of Radiation Medicine and Protection (GZK1201909) and a Project Funded by the Priority Academic Program Development of Jiangsu Higher Education Institutions.

Notes and references

1 H. Sung, J. Ferlay, R. L. Siegel, M. Laversanne, I. Soerjomataram, A. Jemal and F. Bray, *CA Cancer J. Clin.*, 2021, 1–41.
2 P. H. Viale, *J. Adv. Pract. Oncol.*, 2020, **11**, 135–136.
3 S. Spolaor, M. Scheve, M. Firat, P. Cazzaniga, D. Besozzi and M. S. Nobile, *Front. Genet.*, 2021, **12**, 617935.
4 J. Y. Zhang, Y. Y. Yan, J. J. Li, R. Adhikari and L. W. Fu, *Front. Pharmacol.*, 2020, **11**, 722.
5 H. Kang and J. S. Kauh, *Curr. Treat. Options Oncol.*, 2011, **12**, 96–106.
6 M. Leary, S. Heerboth, K. Lapinska and S. Sarkar, *Cancers*, 2018, **10**, 483.
7 R. X. Zhang, H. L. Wong, H. Y. Xue, J. Y. Eoh and X. Y. Wu, *J. Controlled Release*, 2016, **240**, 489–503.
8 J. Nam, S. Son, K. S. Park, W. Zou, L. D. Shea and J. J. Moon, *Nat. Rev. Mater.*, 2019, **4**, 398–414.
9 X. Zeng, M. Luo, G. Liu, X. Wang, W. Tao, Y. Lin, X. Ji, L. Nie and L. Mei, *Adv. Sci.*, 2018, **5**, 1800510.
10 F. Zhang, G. Lu, X. Wen, F. Li, X. Ji, Q. Li, M. Wu, Q. Cheng, Y. Yu, J. Tang and L. Mei, *J. Controlled Release*, 2020, **326**, 131–139.
11 R. F. Ozols, *Ann. Oncol.*, 2006, **17**(5), 181–187.
12 R. M. Navari and M. Aapro, *N. Engl. J. Med.*, 2016, **374**, 1356–1367.
13 A. Pearce, M. Haas, R. Viney, S. A. Pearson, P. Haywood, C. Brown and R. Ward, *PLoS One*, 2017, **12**, e0184360.
14 Y. J. Cheng, J. J. Hu, S. Y. Qin, A. Q. Zhang and X. Z. Zhang, *Biomaterials*, 2020, **232**, 119738.
15 W. He, Y. Jiang, Q. Li, D. Zhang, Z. Li and Y. Luan, *Acta Biomater.*, 2019, **84**, 356–366.
16 J. Liu, F. Zhai, H. Zhou, W. Yang and S. Zhang, *Adv. Healthcare Mater.*, 2019, **8**, e1801300.

17 Z. Zhang, J. Wang and C. Chen, *Adv. Mater.*, 2013, **25**, 3869–3880.
18 K. D. Barnes, G. Shafirstein, J. S. Webber, N. A. Koonce, Z. Harris and R. J. Griffin, *Int. J. Hyperthermia*, 2013, **29**, 474–479.
19 C. W. Song, H. J. Park, C. K. Lee and R. Griffin, *Int. J. Hyperthermia*, 2005, **21**, 761–767.
20 M. R. Dreher, W. Liu, C. R. Michelich, M. W. Dewhirst, F. Yuan and A. Chilkoti, *J. Natl. Cancer Inst.*, 2006, **98**, 335–344.
21 R. J. Griffin, R. P. Dings, A. Jamshidi-Parsian and C. W. Song, *Int. J. Hyperthermia*, 2010, **26**, 256–263.
22 J. H. Baek, J. H. Lee, R. Valcavi, C. M. Pacella, H. Rhim and D. G. Na, *Korean J. Radiol.*, 2011, **12**, 525–540.
23 A. C. Schmitz, D. Gianfelice, B. L. Daniel, W. P. Mali and M. A. van den Bosch, *Eur. Radiol.*, 2008, **18**, 1431–1441.
24 Y. Yu, D. Tang, C. Liu, Q. Zhang, L. Tang, Y. Lu and H. Xiao, *Adv. Mater.*, 2022, **34**, e2105976.
25 J. Li, W. Zhang, W. Ji, J. Wang, N. Wang, W. Wu, Q. Wu, X. Hou, W. Hu and L. Li, *J. Mater. Chem. B*, 2021, **9**, 7909–7926.
26 L. Cheng, C. Wang, L. Feng, K. Yang and Z. Liu, *Chem. Rev.*, 2014, **114**, 10869–10939.
27 D. Zhi, T. Yang, J. O'Hagan, S. Zhang and R. F. Donnelly, *J. Controlled Release*, 2020, **325**, 52–71.
28 J. Chen, C. Ning, Z. Zhou, P. Yu, Y. Zhu, G. Tan and C. Mao, *Prog. Mater. Sci.*, 2019, **99**, 1–26.
29 Z. Li, Y. Yang, H. Wei, X. Shan, X. Wang, M. Ou, Q. Liu, N. Gao, H. Chen, L. Mei and X. Zeng, *J. Controlled Release*, 2021, **338**, 719–730.
30 X. Liang, X. Ye, C. Wang, C. Xing, Q. Miao, Z. Xie, X. Chen, X. Zhang, H. Zhang and L. Mei, *J. Controlled Release*, 2019, **296**, 150–161.
31 T. Chen, W. Zeng, C. Tie, M. Yu, H. Hao, Y. Deng, Q. Li, H. Zheng, M. Wu and L. Mei, *Bioact. Mater.*, 2022, **10**, 515–525.
32 M. Ou, C. Lin, Y. Wang, Y. Lu, W. Wang, Z. Li, W. Zeng, X. Zeng, X. Ji and L. Mei, *J. Controlled Release*, 2022, **345**, 755–769.
33 X. Cheng, Y. Yong, Y. Dai, X. Song, G. Yang, Y. Pan and C. Ge, *Theranostics*, 2017, **7**, 4087–4098.
34 C. Cui, J. Li, J. Fang, Y. Zhao, Y. Zhang, S. Ye, A. Wang, Y. Feng, Q. Mao, H. Qin and H. Shi, *Chin. Chem. Lett.*, 2022, **33**, 3478–3483.
35 E. Boisselier and D. Astruc, *Chem. Soc. Rev.*, 2009, **38**, 1759–1782.
36 Y. N. Xia, W. Y. Li, C. M. Cobley, J. G. Chen, X. H. Xia, Q. Zhang, M. X. Yang, E. Cho and P. K. Brown, *Acc. Chem. Res.*, 2011, **44**, 914–924.
37 X. Cheng, X. Tian, A. Wu, J. Li, J. Tian, Y. Chong, Z. Chai, Y. Zhao, C. Chen and C. Ge, *ACS Appl. Mater. Interfaces*, 2015, **7**, 20568–20575.
38 N. Gupta and R. Malviya, *Biochim. Biophys. Acta, Rev. Cancer*, 2021, **1875**, 188532.
39 N. S. Abadeer and C. J. Murphy, *J. Phys. Chem. C*, 2016, **120**, 4691–4716.
40 S. Ruan, C. Hu, X. Tang, X. Cun, W. Xiao, K. Shi, Q. He and H. Gao, *ACS Nano*, 2016, **10**, 10086–10098.
41 Y. Ma, J. Hong and Y. Ding, *Adv. Healthcare Mater.*, 2020, **9**, e1901448.
42 X. Cheng, X. Zhou, J. Xu, R. Sun, H. Xia, J. Ding, Y. E. Chin, Z. Chai, H. Shi and M. Gao, *Anal. Chem.*, 2021, **93**, 9277–9285.
43 H. Li, X. Liu, N. Huang, K. Ren, Q. Jin and J. Ji, *ACS Appl. Mater. Interfaces*, 2014, **6**, 18930–18937.
44 R. Zhang, L. Wang, X. Wang, Q. Jia, Z. Chen, Z. Yang, R. Ji, J. Tian and Z. Wang, *Adv. Healthcare Mater.*, 2020, **9**, e2000394.
45 S. Kang, S. H. Bhang, S. Hwang, J. K. Yoon, J. Song, H. K. Jang, S. Kim and B. S. Kim, *ACS Nano*, 2015, **9**, 9678–9690.
46 J. Nam, N. Won, H. Jin, H. Chung and S. Kim, *J. Am. Chem. Soc.*, 2009, **131**, 13639–13645.
47 K. Yang, Y. Liu, Y. Wang, Q. Ren, H. Guo, J. B. Matson, X. Chen and Z. Nie, *Biomaterials*, 2019, **223**, 119460.
48 Y. Zhang, J. Chang, F. Huang, L. Yang, C. Ren, L. Ma, W. Zhang, H. Dong, J. Liu and J. Liu, *ACS Biomater. Sci. Eng.*, 2019, **5**, 1589–1601.
49 S. Ruan, W. Xiao, C. Hu, H. Zhang, J. Rao, S. Wang, X. Wang, Q. He and H. Gao, *ACS Appl. Mater. Interfaces*, 2017, **9**, 20348–20360.
50 C. J. Kim, D. I. Lee, C. Kim, K. Lee, C. H. Lee and I. S. Ahn, *Anal. Chem.*, 2014, **86**, 3825–3833.
51 F. Wen, Y. Dong, L. Feng, S. Wang, S. Zhang and X. Zhang, *Anal. Chem.*, 2011, **83**, 1193–1196.
52 Q. Mao, J. Fang, A. Wang, Y. Zhang, C. Cui, S. Ye, Y. Zhao, Y. Feng, J. Li and H. Shi, *Angew. Chem., Int. Ed.*, 2021, **60**, 23805–23811.
53 Z. He, A. Zhong, H. Zhang, L. Xiong, Y. Xu, T. Wang, M. Zhou and K. Huang, *Chemistry*, 2015, **21**, 10220–10225.
54 M. Sun, F. Liu, Y. Zhu, W. Wang, J. Hu, J. Liu, Z. Dai, K. Wang, Y. Wei, J. Bai and W. Gao, *Nanoscale*, 2016, **8**, 4452–4457.
55 X. Cheng, R. Sun, L. Yin, Z. Chai, H. Shi and M. Gao, *Adv. Mater.*, 2017, **29**, 1604894.
56 T. Bian, L. Shang, H. Yu, M. T. Perez, L. Z. Wu, C. H. Tung, Z. Nie, Z. Tang and T. Zhang, *Adv. Mater.*, 2014, **26**, 5613–5618.
57 S. Das, P. Ranjan, P. S. Maiti, G. Singh, G. Leitus and R. Klajn, *Adv. Mater.*, 2013, **25**, 422–426.
58 J. Lai, Y. Xu, X. Mu, X. Wu, C. Li, J. Zheng, C. Wu, J. Chen and Y. Zhao, *Chem. Commun.*, 2011, **47**, 3822–3824.
59 Y. Shiraishi, K. Tanaka, E. Shirakawa, Y. Sugano, S. Ichikawa, S. Tanaka and T. Hirai, *Angew. Chem., Int. Ed.*, 2013, **52**, 8304–8308.
60 J. Xu, X. Cheng, F. Chen, W. Li, X. Xiao, P. Lai, G. Xu, L. Xu and Y. Pan, *J. Mater. Sci. Technol.*, 2021, **63**, 97–105.
61 X. Ding, C. H. Liow, M. Zhang, R. Huang, C. Li, H. Shen, M. Liu, Y. Zou, N. Gao, Z. Zhang, Y. Li, Q. Wang, S. Li and J. Jiang, *J. Am. Chem. Soc.*, 2014, **136**, 15684–15693.
62 H. Xia, Y. Gao, L. Yin, X. Cheng, A. Wang, M. Zhao, J. Ding and H. Shi, *ChemBioChem*, 2018, **20**, 667–671.

63 W. Song, Y. Wang, J. Qu, M. M. Madden and Q. Lin, *Angew. Chem., Int. Ed.*, 2008, **47**, 2832–2835.
64 S. Pan, S. Y. Jang, D. Wang, S. S. Liew, Z. Li, J. S. Lee and S. Q. Yao, *Angew. Chem., Int. Ed.*, 2017, **56**, 11816–11821.
65 A. R. Badireddy, M. R. Wiesner and J. Liu, *Environ. Sci. Technol.*, 2012, **46**, 10081–10088.
66 O. S. Kwon, B. Kwon, J. Kim and B. H. Kim, *Asian Nurs. Res.*, 2022, **16**, 73–79.
67 B. Clares, R. A. Biedma-Ortiz, E. Saez-Fernandez, J. C. Prados, C. Melguizo, L. Cabeza, R. Ortiz and J. L. Arias, *Eur. J. Pharm. Biopharm.*, 2013, **85**, 329–338.
68 W. Guo, F. Wang, D. Ding, C. Song, C. Guo and S. Liu, *Chem. Mater.*, 2017, **29**, 9262–9274.
69 H. Song, T. Peng, X. Wang, B. Li, Y. Wang, D. Song, T. Xu and X. Liu, *Front. Chem.*, 2022, **10**, 842682.
70 C. Yang, C. Guo, W. Guo, X. Zhao, S. Liu and X. Han, *ACS Appl. Nano Mater.*, 2018, **1**, 820–830.